Synthesis of Calcium Phosphate Nanofilaments in Reverse Micelles

Sajanikumari Sadasivan,[†] Deepa Khushalani,[‡] and Stephen Mann*,[†]

Centre for Organized Matter Chemistry, School of Chemistry, University of Bristol, Bristol BS8 1TS, United Kingdom, and Department of Chemical Sciences, Tata Institute of Fundamental Research, Colaba, Mumbai, India, 400005

Received November 29, 2004. Revised Manuscript Received March 4, 2005

Reverse micelles of calcium bis(2-ethylhexyl)phosphate ($Ca(DEHP)_2$) were used to synthesize calcium phosphate nanostructures from a reaction mixture initially containing a water-in-cyclohexane emulsion of $Ca(DEHP)_2$, ammonium hydrogen phosphate, and triblock copolymer, P123. Bundles of DEHP-coated amorphous calcium phosphate nanofilaments, 2 nm in width and >300 μm in length were formed in the oil layer of a phase-separated reaction mixture prepared at a $[Ca]:[PO_4]$ molar ratio of 1:1 and pH of 8.2. The nanofilament bundles were stable in the reverse micelle phase up to around 5 days, after which they transformed into 5-nm-wide surfactant-coated hydroxyapatite nanorods. In contrast, similar experiments at a higher supersaturation level (pH = 9, $[Ca]:[PO_4] = 1.66$) produced discrete nanofilaments ($100-500 \times 10-15$ nm in size) that consisted of a linear superstructure based on the side-on stacking of surfactant-coated amorphous calcium phosphate nanorods. Possible factors giving rise to these ordered nanostructures are discussed.

Introduction

Bioinorganic materials such as bones, shells, and teeth exhibit remarkable levels of structural and functional complexity that are determined across multiple length scales by organic matrix-mediated biomineralization.[1] This process principally involves the use of organic macromolecular assemblies to control various key aspects of inorganic deposition from supersaturated biological solutions. In particular, the organic matrix plays an important role in delineating the structure and chemistry of the mineralization environment, providing site-specific nucleation centers, regulating crystal growth and morphological expression, and facilitating the construction of higher-order assemblies.[2] Given the complexity and interactive nature of these multiple functions, it is no surprise that biominerals formed by organic-matrix mediation are often disparate in structure, composition, and function. For example, deposition of calcium phosphate (carbonated hydroxyapatite, $Ca_6(PO_4)_{10}(OH)_2$) in bone and tooth enamel is intimately associated with protein-based matrixes (collagen and amelogenin, respectively), but whereas the primary particles in bone are in the form of nanoscopic platelike hydroxyapatite crystals, those in tooth enamel are highly elongated nanofilaments.[3] Significantly, in both cases the hydroxyapatite primary nanostructures are employed as building blocks for the long-range assembly of macroscopic materials with hierarchical order.

Understandably, the ability to prepare synthetic calcium phosphate materials with levels of structural, morphological, and organizational complexity analogous to their organic matrix-mediated counterparts has not yet been attained. However, because synthetic calcium phosphates have important industrial and biomedical uses, significant progress has been made for example in controlling crystal morphology using water soluble organic additives such as polyaspartic acid,[4] poly(acrylic acid),[5] and monosaccharides.[6] Similarly, ionic,[7−9] nonionic,[10] and block-copolymer[11] surfactants have been used to produce calcium phosphates with specific and often unusual morphologies. In other studies, self-assembled organic supramolecular structures have been employed as templates for the controlled deposition of calcium phosphate. For example, lipid vesicles[12] (liposomes) and amphiphilic peptides[13] were used to prepare calcium phosphate nanoshells and nanofibers, respectively. Likewise, biopolymer templates in the form of cellulose[14] or collagen fibrils[15] have been used to prepare organized calcium phosphate containing composites from aqueous solutions.

Although the above examples clearly highlight the importance of organic structure-directing agents in mediating

* To whom correspondence should be addressed. Email: s.mann@bris.ac.uk.
[†] University of Bristol.
[‡] Tata Institute of Fundamental Research.

(1) Lowenstam, H. A.; Weiner, S. *On Biomineralization*; Oxford University Press: NewYork, 1989.
(2) Mann, S. *Biomineralization: Principles and Concepts in Bioinorganic Materials Chemistry*; Oxford University Press: Oxford, U.K., 2001.
(3) Weiner, S. *CRC Crit. Rev. Biochem.* **1986**, *20*, 365.
(4) (a) Burke, E. M.; Guo, Y.; Colon, L.; Rahima, M.; Veis, A.; Nancollas, G. H. *Colloids Surf., B* **2000**, *17*, 49. (b) Bigi, A.; Boanini, E.; Walsh, D.; Mann, S. *Angew. Chem., Int. Ed.* **2002**, *41*, 2163.
(5) Bettoni, E.; Bigi, A.; Falini, G.; Panzavolta, S.; Roveri, N. *J. Mater. Chem.* **1999**, *9*, 779.
(6) Walsh, D.; Kingston, J. L.; Heywood, B. R.; Mann, S. *J. Cryst. Growth* **1993**, *133*, 1.
(7) Sarda, S.; Heughebaert, M.; Lebugle, A. *Chem. Mater.* **1999**, *11*, 2722.
(8) Bujan, M.; Sikiric, M.; Vincekovic, F.; Vdovic, N.; Garti, N.; Milhofer, F. H. *Langmuir* **2001**, *17*, 6461.
(9) Hovarth, L.; Smit, I.; Sikiric, M.; Vincekovic, F. *J. Cryst. Growth* **2000**, *219*, 91.
(10) Qi, L.; Ma, J.; Cheng, H.; Zhao, Z. *J. Mater. Sci. Lett.* **1997**, *16*, 1779.
(11) Antonietti, M.; Breulmann, M.; Goltner, C.; Colfen, H.; Wong, K.; Walsh, D.; Mann, S. *Chem.−Eur. J.* **1998**, *4*, 2493.
(12) Schmidt, H. A.; Ostafin, A. E. *Adv. Mater.* **2002**, *14*, 532.
(13) Hartgerink, J. D.; Beniash, E.; Stupp, S. I. *Science* **2001**, *294*, 1684.
(14) Yokogawa, Y.; Toriyama, M.; Kawamoto, Y.; Nishizawa, K.; Kameyama, T.; Okada, K.; Okuyama, M. *J. Mater. Res.* **1998**, *13*, 922.
(15) Zhang, W.; Liao, S. S.; Cui, F. Z. *Chem. Mater.* **2003**, *15*, 3221.

10.1021/cm047926g CCC: $30.25
Published on Web 04/15/2005

Chart 1. Calcium Bis(2-ethylhexyl)phosphate ($Ca(DEHP)_2$)

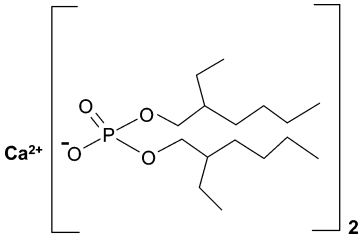

spatial and crystallochemical aspects of calcium phosphate deposition, such processes are usually undertaken in bulk aqueous media with the consequence that the efficacy of these templates is often critically dependent on solution properties such as supersaturation, ionic strength, and pH. Significantly, the interplay between organic matrix- and environment-mediated processes becomes highly pronounced when the deposition of the inorganic phase is confined to nanometer length scales, for instance by undertaking reactions in supersaturated water-in-oil microemulsion droplets.[16] These oil-based systems are stabilized by organic surfactants and contain only limited amounts of water, with the consequence that inorganic nucleation and growth are strongly coupled with the local properties of the reaction media to produce for example microskeletal calcium phosphate frameworks,[17] linear chains of $BaCrO_4$ nanoparticles,[18] as well as a variety of nanofilament-based superstructures.[19] Generally, these self-assembled nanostructures are formed by emergent processes that involve time-dependent mesoscale transformations of surfactant-coated amorphous inorganic nanoparticles[16] and which are highly sensitive to reactant molar ratio, number ratio of water droplets per nanoparticle, and droplet size. In particular, complex nanostructures tend to be produced at relatively low w values ($w = [H_2O]/[\text{surfactant}] = 5-10$), often just above that required for reverse micelle bulk hydration ($w > 3.5$).

In this paper, we extend the above approach to the reverse micelle-based synthesis of calcium phosphate hybrid nanostructures in the form of discrete or coaligned surfactant-coated nanofilaments. We use the highly hydrophobic calcium salt of bis(2-ethylhexyl)phosphoric acid ($Ca(DEHP)_2$, Chart 1) in place of the more conventional surfactant, bis(2-ethylhexyl)sulfosuccinate (AOT), to generate an interface that is compatible specifically with the nucleation of calcium phosphate. Previous studies have used an analogous surfactant, calcium dodecyl phosphate, as a mesolamellar solid phase for the organized nucleation and growth of calcium phosphate,[20] whereas dispersed reaction media are investigated in this paper. Significantly, even though the headgroup areas are effectively unchanged (~0.65 nm^2), replacing the sulfosuccinate headgroup of AOT by a phosphate moiety severely limits the amount of water sequestered by the reverse micelles, as demonstrated by neutron scattering investigations.[21] For example, these studies showed that the formation of hydrated reverse micelles of $Ca(DEHP)_2$ as short cylindrical aggregates, ca. 2×15 nm in size, was unaffected by the addition of excess water. Thus, under these conditions, calcium phosphate deposition in the oil phase is expected to be strongly influenced by interactions at the surfactant-inorganic interface and moreover restricted to the nanometer length scale by confinement within the reverse micelle aggregates.

Here, we demonstrate this principle using a reaction mixture prepared by adding solid $Ca(DEHP)_2$ to a stirred water-in-cyclohexane emulsion containing ammonium hydrogen phosphate and poly(ethylene oxide)−polypropyleneoxide−poly(ethylene oxide) triblock copolymer, P123. Extraction of hydrated HPO_4^{2-} anions from the emulsion gives rise to calcium phosphate nucleation within the oil-soluble DEHP reverse micelles, while ion-exchange-mediated transfer of Ca^{2+} from $Ca(DEHP)_2$ into the water phase results in bulk inorganic precipitation. In addition, the mineralized structures are readily separated by spontaneous demixing of the unstirred reaction solution into upper and lower oil and water layers, respectively. As the products obtained in the phase-separated water layer were typical in terms of known calcium phosphate structures and morphology, this paper focuses explicitly on the growth and form of nanostructured materials produced in association with reverse micelles present in the oil-based reaction media.

Experimental Section

Materials. All chemicals were of analytical grade and used without further purification.

Preparation of Calcium Bis(2-ethylhexyl)phosphate. $Ca(DEHP)_2$ was prepared by ion exchange of bis(2-ethylhexyl)phosphoric acid (HDEHP).[21] $Ca(OH)_2$ was freshly prepared by mixing 15 mL of 1 M $Ca(NO_3)_2$ and 20 mL of 1 M NaOH. The precipitated $Ca(OH)_2$ was filtered and thoroughly washed with water to remove excess NaOH and then added directly to a biphasic system containing water (50 mL) and a solution of HDEHP in diethyl ether in a separating funnel (25 mL, 0.75 M). The resulting mixture was thoroughly shaken and left to phase separate overnight. The lower aqueous phase was then removed, together with any excess calcium hydroxide present at the interface. The upper ether layer was concentrated using a rotary evaporator to obtain a viscous gel of $Ca(DEHP)_2$ that was used as prepared for reverse micelle experiments. Analytical data for $Ca(DEHP)_2$: ^{31}P liquid ($CDCl_3$) NMR spectroscopy; single resonance, $\delta = -1.66$ (HDEHP $\delta = 1.82$). Fourier transform IR (FTIR) spectroscopy; 2900−2800 cm^{-1} (C−H str), 1460−1350 cm^{-1} (C−H def), 875 cm^{-1} (P−O sym. str.), 1033 cm^{-1} (P−O antisym. str.), 521 cm^{-1} (O−P−O antisym. bend.), 1218 cm^{-1} (P═O), 1033 cm^{-1} (P−[O−C]), 778 cm^{-1} ([P−O]−C). Thermal gravimetric analysis (TGA); 70wt % loss between 200 and 300 °C, (HDEHP, 74 wt %). Differential thermal gravimetry (DTG); decomposition temperature, 263 °C (HDEHP, 236 °C). Powder X-ray diffraction (PXRD) reflections; lamellar phase, 1.62 (001), 0.8 (002), 0.54 (003) nm.

(16) Coelfen, H.; Mann, S. *Angew. Chem., Int. Ed.* **2003**, *42*, 2350.
(17) (a) Walsh, D.; Hopwood, J. D.; Mann, S. *Science* **1994**, *264*, 1576. (b) Walsh, D.; Mann, S. *Chem. Mater.* **1996**, *8*, 1944.
(18) (a) Li, M.; Schnablegger, H.; Mann, S. *Nature*, **1999**, *402*, 393. (b) Johnson, C. J.; Li, M.; Mann S. *Adv. Funct. Mater.* **2004**, in press.
(19) (a) Hopwood, J.; Mann, S. *Chem. Mater.* **1997** *9*, 1819. (b) Qi, L.; Ma, J.; Cheng, H.; Zhao, Z. *J. Phys. Chem. B* **1997**, *101*, 3460. (c) Rees, G. D.; Evans-Gowing, R.; Hammond, S. J. Robinson, B. H. *Langmuir*, **1999**, *15*, 1993. (d) Li, M.; Mann, S. *Langmuir* **2000**, *16*, 7088. (e) Li, M.; Mann, S. *Adv. Funct. Mater.* **2002**, *12*, 773. (f) Li, M.; Lebeau, B.; Mann, S. *Adv. Mater.* **2003**, *15*, 2032.
(20) (a) Ozin, G. A.; Varaksa, N.; Coombs, N.; Davies, J. E.; Perovic, D.; Ziliox, M. *J. Mater. Chem.* **1997**, *7*, 1601. (b) Soten, I.; Ozin, G. A. *J. Mater. Chem.* **1999**, *9*, 703.
(21) Steyler, D.; Jenta, T. R.; Robinson, B. H.; Eastoe, J.; Heenan, R. K. *Langmuir* **1996**, *12*, 1483.

Reverse Micelle-Based Synthesis of Calcium Phosphate Nanofilaments. Calcium phosphate nanofilaments were synthesized in reverse micelles at a [Ca]:[PO_4] molar ratio of 1:1 and pH value of 8.2. In a typical synthesis, P123 (0.2 g, 3.5×10^{-5} mol) was dispersed in 5 g of cyclohexane, stirred overnight, and then sonicated for 1 min using a probe sonicator to produce a homogeneous opaque solution. To this was added 2 mL of aqueous ammonium hydrogen phosphate (0.36 M, pH 8.15), and the mixture sonicated for 1 min to produce a milky white emulsion. $Ca(DEHP)_2$ (0.5 g, 7.7×10^{-4} mol) was then added and the mixture stirred for 1 h, after which the stirring was stopped and the quiescent mixture left to separate into a transparent reverse micelle upper layer and a lower layer consisting of a water-rich gel-like phase.

Samples for analysis were collected at various time intervals from both the upper and lower layers of the biphasic mixture. For TEM, a drop from the upper or lower layer was dispersed in cyclohexane (0.5 mL) or ethanol (0.5 mL), respectively, and a drop of the diluted samples air dried onto carbon-coated copper grids, followed by washing the grids in cyclohexane or ethanol, respectively, and air drying. TEM was performed in bright field mode using a JEOL 1200 electron microscope operating at 120 kV. EDX analysis was used to confirm the presence of certain elements and selected area electron diffraction (SAED) used to identify the calcium phosphate phase. For FTIR spectroscopy, samples were washed with cyclohexane or ethanol and air dried and then analyzed using KBr disks. Samples for TGA were prepared by washing and air drying and then heated from 25 to 800 °C at a rate of 5 °C/min using a Simultaneous Thermal Analysis STA 409EP.

Experiments were undertaken as described above except that the pH of the starting emulsion was raised to 9 by addition of 4 M NH_4OH and the ammonium hydrogen phosphate concentration reduced to 0.22 M to give an increased [Ca]:[PO_4] molar ratio of 1.66:1. The reaction mixture separated on standing to give a transparent reverse micelle upper layer and a lower water-rich gel-like phase. Samples were collected from both layers and analyzed as described above.

Control experiments based on the above synthesis method at pH 8.2 and [Ca]:[PO_4] = 1:1 but in the absence of P123 were undertaken. Under these conditions, the reaction mixture separated into three 3 phases: a transparent reverse micelle upper layer, a thin gel-like middle layer, and a clear bottom aqueous layer. Similarly, control experiments were carried out by replacing $Ca(DEHP)_2$ with $CaCl_2$ (0.0816 g, 7.4×10^{-4} mol) at a [Ca]:[PO_4] molar ratio of 1:1 and pH = 8.2. In this case, the mixture separated into a transparent oil/P123 upper layer and gel-like water-rich lower phase when left unstirred.

Results

Reaction mixtures comprising aqueous $(NH_4)_2HPO_4$, $Ca(DEHP)_2$, P123, and cyclohexane were prepared at a [Ca]:[PO_4] molar ratio of 1:1 and pH of 8.2, and stirred for 1 h. When left unstirred at room temperature, the mixtures separated into upper and lower layers consisting of a transparent reverse micelle phase and gel-like aqueous phase, respectively. TEM images of samples extracted from the upper layer after 2 days revealed bundles of coaligned electron dense filaments that were variable in length (typically > 300 nm) but highly uniform in width (2 nm) (Figure 1). EDX analysis on the nanofilament bundles showed peaks for calcium (K_α 3.70, K_β 4.01 keV) and phosphorus (K_α 2.01 keV), and selected area electron diffraction, as well as PXRD data obtained from dried and washed bulk samples, indicated

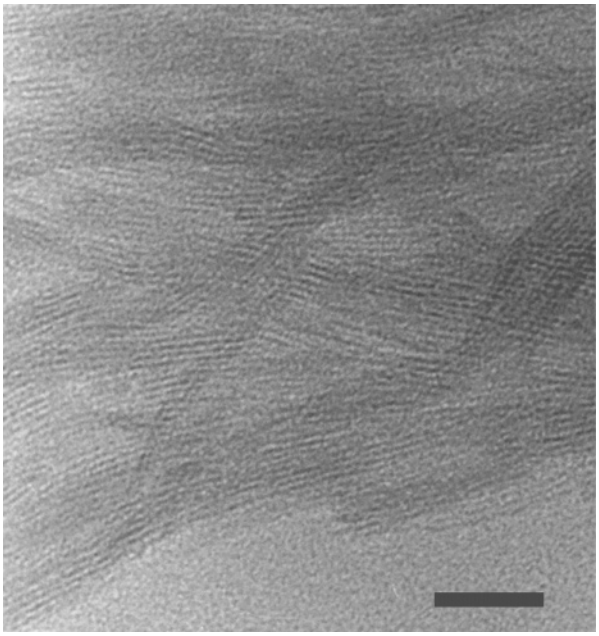

Figure 1. TEM image showing bundles of coaligned 2-nm-wide calcium phosphate nanofilaments prepared in $Ca(DEHP)_2$ reverse micelles at [Ca]:[PO_4] = 1:1 and pH = 8.2. The nanofilaments appear in the image as thin electron dense lines and are separated by a uniform spacing of 1.5 nm. Scale bar = 50 nm.

that the filaments were amorphous. In contrast, analogous studies on samples extracted from the aqueous lower layer showed the presence of well-defined hydroxyapatite single crystals with characteristic needlelike morphology with a mean length and width of 965 (σ = 85) and 48 (σ = 13) nm, respectively (data not shown). Nanofilament-based superstructures were also absent in samples extracted from the upper oil layer associated with $Ca(DEHP)_2$/P123/H_2O/cyclohexane mixture prepared in the absence HPO_4^{2-} ions, or when $Ca(DEHP)_2$ was replaced by aqueous $CaCl_2$ in phosphate-containing P123/cyclohexane/H_2O reaction mixtures.

Significantly, as shown in Figure 1, the coaligned nanofilaments were separated by an electron-opaque region with a constant spacing of 1.5 nm. This spacing was in agreement with the interlayer distance (d_{001} = 1.6 nm) determined by PXRD for a pure $Ca(DEHP)_2$ lamellar mesophase and suggested that a bilayer of DEHP molecules was present between adjacent nanofilaments. This was consistent with FTIR spectra of washed and dried nanofilaments (Figure 2), which showed CH (2900−2800, 1300−1400 cm^{-1}) and P−O−C (1215, 778 cm^{-1}) bands associated with DEHP, as well as broad peaks for inorganic phosphate at 1020−1100 cm^{-1} (ν_3PO_4 anti-sym str.) and 556 cm^{-1} (ν_4PO_4 anti-sym def.). TGA profiles of the washed calcium phosphate nanofilaments also indicated that surfactant molecules were intimately associated with the nanofilaments (Figure 3). A weight loss of 10% was detected between 200 and 400 °C with a corresponding peak in the DTG curve at 240 °C. These were attributed primarily to the decomposition of DEHP rather than P123 as TGA plots for nanofilament samples prepared in the absence of P123 showed a similar weight loss (8.5%) between 200 and 400 °C. Together, the above data were consistent with the reverse micelle mediated

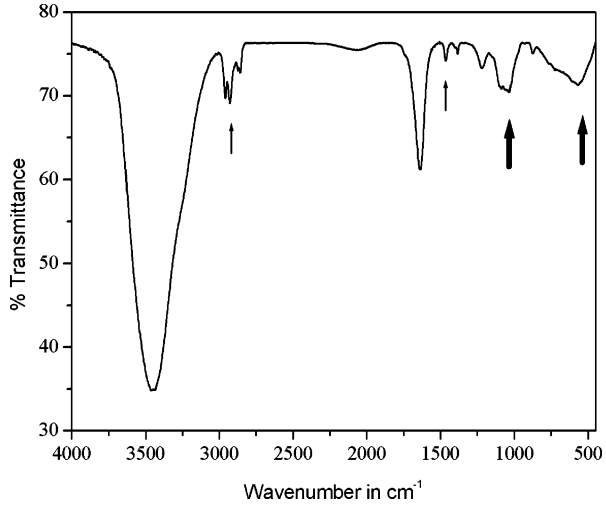

Figure 2. FTIR spectra of washed/dried calcium phosphate nanofilaments showing absorption bands associated with inorganic phosphate (bold arrows) and DEHP surfactant (small arrows).

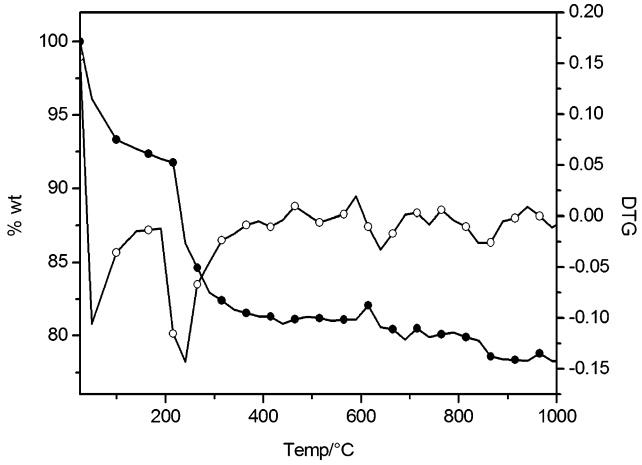

Figure 3. TGA of calcium phosphate nanofilaments showing changes in wt % (filled circles) and corresponding DSC (DTG) curve (open circles) for temperatures up to 1000 °C.

synthesis of coaligned bundles of 2-nm-wide nanofilaments of amorphous calcium phosphate in association with a surrounding cylindrical shell of strongly bound DEHP molecules.

Other studies were undertaken to investigate the influence of reaction conditions on nanofilament formation and to determine the time-dependent properties of these nanomaterials. TEM images of samples extracted after 2 days from the separated upper layer of reaction mixtures prepared at a higher supersaturation level (pH = 9, [Ca]:[PO_4] = 1.66) showed the presence of discrete nanofilaments that were longer and wider than those formed at pH 8.2. The filaments were up to 100−500 and 10−15 nm in length and width, respectively, and exhibited irregular edges that appeared to consist of fine striations running normal to the filament axis (Figure 4). No bundled superstructures were observed, although the nanofilaments did self-assemble when dried onto the TEM grid into discrete pairs that were aligned in parallel with a constant spacing of ca. 1.5 nm (Figure 4). EDX analysis and electron diffraction confirmed that the nanofilaments consisted of amorphous calcium phosphate, and FTIR spectroscopy and TGA showed that DEHP molecules were

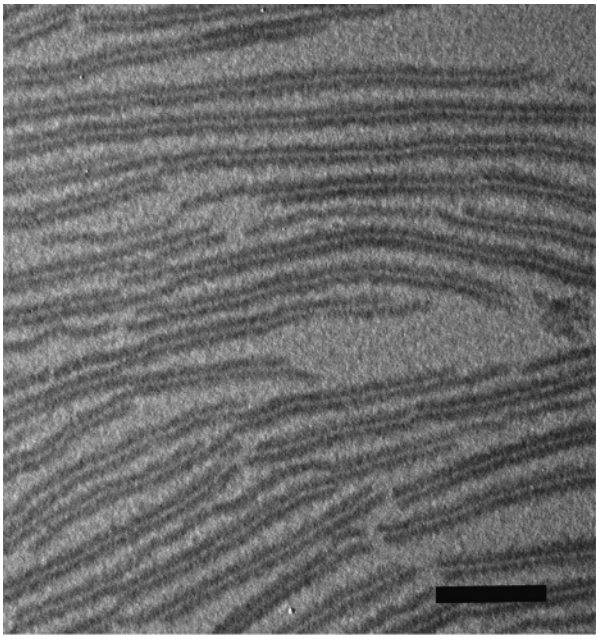

Figure 4. Low magnification image showing showing pairwise aggregation of amorphous calcium phosphate nanofilaments prepared in $Ca(DEHP)_2$ reverse micelles at pH = 9 and [Ca]:[PO_4] = 1.66. Scale bar = 100 nm.

strongly associated with nanostructures. Formation of the 10−15-nm-wide nanofilaments was dependent on the increase in supersaturation associated with the relatively high pH of 9 used in the reaction mixture, rather than the change in molar ratio, as other studies undertaken at a pH of 8.2 but same molar ratio ([Ca]:[PO_4] = 1.66:1) produced 2-nm-wide nanofilaments with homogeneous internal structure.

Significantly, high-resolution TEM images occasionally revealed the presence of lattice fringes that were spaced periodically at a distance of 2 ± 0.3 nm and oriented perpendicular to the nanofilament axis (Figure 5). The fringes were observed throughout the nanofilaments although they were highly susceptible to electron beam damage. The data suggested that each nanofilament was constructed from the side-on stacking of short cylinders of surfactant-coated calcium phosphate, ca. 10−15 nm in length. Thus, deviations in the alignment of these hybrid nanorods within the stacked superstructure, for example, due to drying of the samples onto the support grid, could account for the striations observed in the low magnification TEM images. Moreover, the presence of a uniform spacing of 1.5 nm between pairs of the superstructures suggests that the hemispherical ends of the stacked cylinders fuse on contact to produce a well-defined surfactant bilayer between adjacent filaments. Why this occurs only along one edge of each superstructure is unclear at the present time.

Similar experiments, which were carried out at pH 8.2 and [Ca]:[PO_4] = 1:1 but in the absence of P123, indicated that the triblock copolymer was not primarily responsible for nanofilament formation. Under these conditions, the reaction emulsion separated into three layers, including a clear reverse micelle upper phase. TEM images of samples taken from this layer after 2 days showed amorphous calcium phosphate nanofilaments of similar width (2 nm) and interparticle spacing (1.5 nm) as observed in the presence of P123,

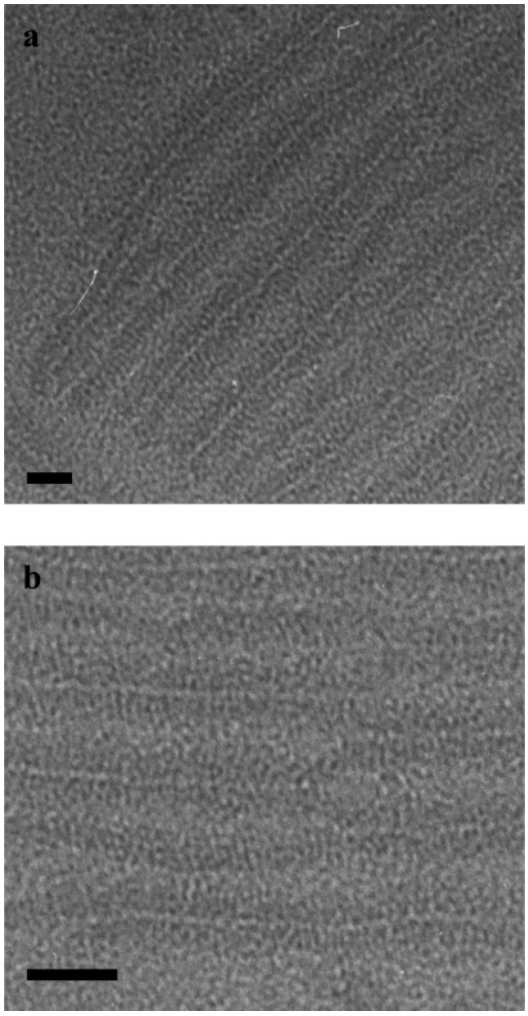

Figure 5. High-resolution TEM images of nanofilaments prepared in Ca(DEHP)$_2$ reverse micelles at pH = 9 and [Ca]:[PO$_4$] = 1.66 showing the presence of 2-nm-spaced lattice fringes running perpendicular to the filament axis. (a) View showing filament tips; the filaments run in parallel from top right to bottom left. (b) View of middle region of filaments; the filaments run in parallel from left to right. The lattice fringes, which are low in contrast, are observed oriented normal to the filament axis in both micrographs. Close contacts between pairs of adjacent filaments are visible as white/light gray lines running parallel to the filament axis. Scale bars = 20 nm.

although the length was reduced (mean length, 130 (σ = 55 nm) and the filament bundles not so well defined.

Time-dependent TEM studies were undertaken at pH 8.2 to elucidate the stages of nanofilament growth. The reaction mixture was stirred for 1 h and then left unstirred for various periods of time. TEM images of samples taken after 10 min from the upper reverse micelle layer showed the presence of discrete 2-nm-sized electron dense spheres along with worm-shaped aggregates that were ca. 2 nm in diameter and 10−40 nm in length and which contained calcium and phosphorus (EDX analysis) (Figure 6a). These structures developed within 2 h into linear nanofilaments that were significantly more rigid and homogeneous in structure (Figure 6b). In addition, the filaments tended to aggregate on the TEM grid into mesostructures with a constant spacing of ca. 1.5 nm, presumably due to the presence of a surrounding shell of DEHP molecules. With time, the length of the filaments continued to increase with no apparent change in the width, and small bundles of periodically spaced

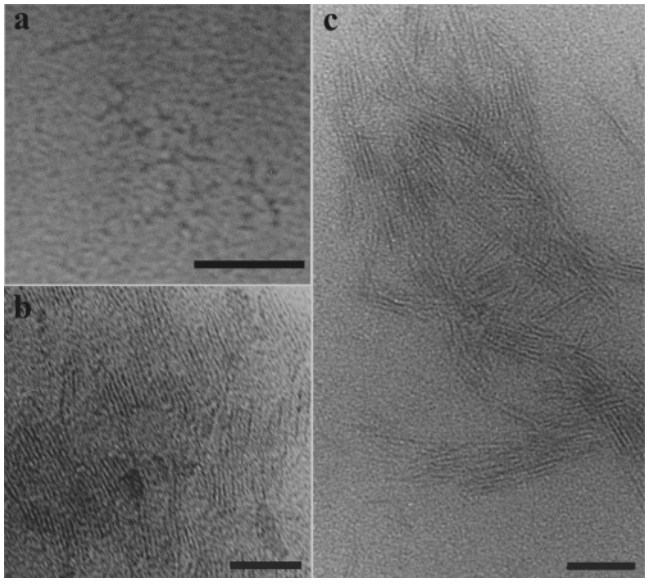

Figure 6. TEM images showing nanofilament development at [Ca]:[PO$_4$] = 1:1 and pH = 8.2. The reaction mixture was stirred for 1 h and then left unstirred for (a) 10 min, (b) 2 h, and (c) 8 h. Nanofilaments imaged in b and c appear as thin electron dense lines, 2 nm in width, and separated by spacing of 1.5 nm. Scale bars = 50 nm.

coaligned filaments were observed after 8 h (Figure 6c). The nanofilament bundles were stable in the reverse micelle phase up to around 5 days, after which they disintegrated initially into spherical structures (mean size, 6 nm (σ = 1.0)) (Figure 7a). Subsequently, these nanoparticles transformed into 5-nm-wide hydroxyapatite nanorods (electron diffraction data: 3.45 (002), 2.77 (112), and 1.76 Å (004)) that remained dispersed in the oil phase, and slowly increased in length from 25 (σ = 1.4) to 38 (σ = 2) nm after 10 and 30 days, respectively (Figure 7b).

The above results indicate that nucleation and growth of calcium phosphate within Ca(DEHP)$_2$ reverse micelles has a marked influence on the structure, morphology, and higher-order assembly of the inorganic phase. Whereas well-defined hydroxyapatite needle-shaped crystals were formed in the aqueous layer of the reaction mixture, highly elongated surfactant-coated amorphous nanofilaments were produced in the oil layer. Transformation of the amorphous phase to crystalline hydroxyapatite was kinetically stabilized over a period of several days, presumably due to exclusion of water molecules by the surfactant overlayer. Moreover, the inability of Ca(DEHP)$_2$ rod-shaped reverse micelles to sequester additional water[21] could account for the nanoscale thickness of the inorganic filaments formed at pH 8.2. However, sequestration of limited amounts of water by the Ca(DEHP)$_2$ reverse micelles must occur as deposition of calcium phosphate requires the transfer of hydrated HPO_4^{2-} ions from the reaction emulsion. One possibility is that cotransfer of monovalent NH_4^+ ions, which maintain electroneutrality during displacement of divalent Ca^{2+} ions from the DEHP headgroups, facilitates small increases in the water content. In this respect, we note that, unlike Ca(DEHP)$_2$, NaDHEP reverse micelles can be hydrated to a w_{max} value of 6,[21] suggesting that similar changes could occur for (NH$_4$)DEHP.

It seems feasible that anisotropic growth of the calcium phosphate nanofilaments is initiated by the rodlike shape of

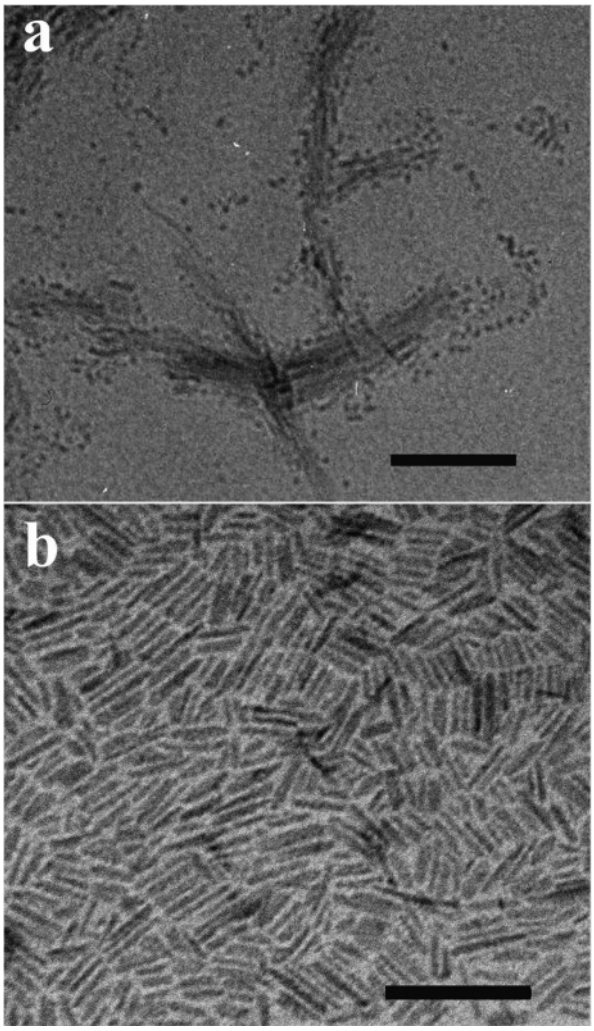

Figure 7. TEM images showing (a) disintegration of nanofilament bundles after 5 days and (b) transformation to hydroxyapatite nanorods after 1 month. Scale bars = 100 nm.

the $Ca(DEHP)_2$ reverse micelles. However, the large disparity in length between these structures (>300 and 15 nm, respectively) indicates a highly cooperative growth mechanism in which both the inorganic and organic components are assembled vectorially along a common direction. This suggests that processes such as ion transfer and micelle fusion occur preferentially at the ends of short rodlike calcium phosphate surfactant primary particles and that DEHP molecules located along the sides of these structures are anchored relatively strongly to the inorganic surface. Such a mechanism implies that the concentration of nonmineralized $Ca(DEHP)_2$ micelles far exceeds the number of primary nanorods, as could be the case when the supersaturation is relatively low at pH = 8.2, and that elongation of the primary particles therefore occurs slowly over several hours along with aggregation of the filaments into bundles. In contrast, the higher rate of primary nucleation associated with the elevated supersaturation level in the reaction mixture prepared at pH = 9 increases the concentration of primary nanorods, with the consequence that ordered aggregation rather than secondary growth occurs. Under these conditions, the surfactant-coated nanorods spontaneously assemble by side-on stacking to produce linear superstructures in the form of elongated filaments with a thickness equivalent to the length of a single primary nanorod.

The spontaneous assembly of nanofilament bundles and nanorod stacks at pH 8.2 and 9, respectively, suggests that there is a significant gain in free energy associated with the formation of an interparticle bilayer of DEHP molecules. The inorganic content associated with the nanofilaments was 90 wt % (TGA results), which was significantly higher than the theoretical value calculated for a closely packed surfactant layer (60 wt %, based on calcium phosphate and DEHP densities of 3.14 and 0.965 g cm^{-3}, respectively), suggesting that the surfactant sheath between adjacent particles was not highly ordered. As discussed in a recent review,[16] adsorption of surfactant molecules onto nanoparticle surfaces can induce ordered aggregation, and this process can become coupled with inorganic crystallization to produce complex mesoscale transformations. Interestingly, while a range of micrometer-sized organized structures are formed in AOT microemulsions by water-induced transformation of surfactant-coated amorphous $BaSO_4$ or $CaCO_3$ nanoparticles,[19] crystallization of hydroxyapatite from DEHP-coated amorphous calcium phosphate produces only discrete nanoparticles, presumably because of the much lower water content associated with $Ca(DEHP)_2$ reverse micelles.

Conclusions

In this paper, we show that reverse micelles of $Ca(DEHP)_2$ can be used to synthesize two different types of calcium phosphate nanostructures from a reaction mixture initially containing a water-in-cyclohexane emulsion of $Ca(DEHP)_2$, ammonium hydrogen phosphate, and triblock copolymer, P123. At a [Ca]:[PO_4] molar ratio of 1:1 and pH of 8.2, bundles of DEHP-coated amorphous calcium phosphate nanofilaments, 2 nm in width and >300 μm in length are formed specifically in the oil layer of the phase-separated reaction mixture, whereas at pH = 9 and [Ca]:[PO_4] = 1.66 discrete nanofilaments ($100-500 \times 10-15$ nm in size) are produced. Significantly, whereas the former are continuous structures that develop by end-on growth of shorter nanofilaments, the latter comprise a linear superstructure based on the side-on stacking of short nanorods of surfactant-coated amorphous calcium phosphate. We attribute these structural variations to differences in the rate of nucleation that influence the concentration of primary particles and hence the driving forces for secondary growth and ordered aggregation. Our results indicate that confinement of calcium phosphate deposition within $Ca(DEHP)_2$ reverse micelles has a marked influence on structure, morphology, and higher-order assembly, suggesting that further exploration of these systems should lead to new types of organized nanomaterials with complex form and architecture for potential application in diverse fields.

CM047926G